

Laboratory Data for X-Ray Astronomy

P. Beiersdorfer¹, G. V. Brown¹, H. Chen¹, M.-F. Gu², S. M. Kahn²
 J. K. Lepson³, D. W. Savin², S. B. Utter¹

¹*High Temperature and Astrophysics Division, Lawrence Livermore National Laboratory*
 7000 East Ave., Livermore, CA 94550, USA

²*Department of Physics, Columbia University, 538 W 120th St., New York, NY 10027, USA*

³*Space Sciences Laboratory, University of California, Berkeley, CA 94720, USA*

Abstract. Laboratory facilities have made great strides in producing large sets of reliable data for X-ray astronomy, which include ionization and recombination cross sections needed for charge balance calculations as well as the atomic data needed for interpreting X-ray line formation. We discuss data from the new generation sources and pay special attention to the LLNL electron beam ion trap experiment, which is unique in its ability to provide direct laboratory access to spectral data under precisely controlled conditions that simulate those found in many astrophysical plasmas. Examples of spectral data obtained in the 1–160 Å wavelength range are given illustrating the type of laboratory X-ray data produced in support of such missions as *Chandra*, *XMM*, *ASCA* and *EUVE*.

1. Introduction

The field of X-ray astronomy has shifted from simple source detection to detailed spectroscopic investigation. The culmination of mapping out X-ray sources came with *ROSAT*, which provided a catalogue of over 60,000 detected sources, covering nearly all categories of X-ray emitting astrophysical objects. Subsequent observations conducted with *ASCA* have demonstrated the great spectral diversity among the different objects. The X-ray band from 0.1 to 10 keV is rich in discrete spectral line emission and comprises the K-shell emission from carbon through nickel, the L-shell emission from neon through nickel, and the M-shell emission from iron and nickel. The *ASCA* observations have thoroughly demonstrated that X-ray emission line spectroscopy represents an indispensable tool for understanding the physical conditions in high-temperature cosmic plasmas.

Although *ASCA* observations provided a wealth of new information, they were limited by the relatively low resolving power of *ASCA*'s energy dispersive instrumentation. Present satellite missions, such as *Chandra* and *XMM*, have overcome this limitation using high-resolution dispersive gratings, and now have the spectral resolution to discern individual spectral features and thus to resolve many of the lines important for plasma diagnostics. This opens the X-ray band to scientific scrutiny in unprecedented fashion.

Successful and reliable interpretation of these X-ray spectra requires an adequate understanding of the atomic data underlying the emission. Cosmic X-ray sources are never in local thermodynamic equilibrium. Calculations of the spectral emission, therefore, must be based on detailed accounting of all microphysical processes that feed and deplete a given quantum level in ions that more often than not have a complex atomic structure. Temperature gradients, transient phenomena, photon fields, flows and shocks further complicate the picture and require atomic data valid also for plasmas outside equilibrium.

The atomic data needs can be grouped into two categories. The first comprises the ionization and recombination data needed for determining the proper ionization structure of the emitting sources. These data determine the relative abundances of each ionization stage of a given element in the plasma. The second comprises the data needed to describe the radiation produced by a given ionization state. These data determine what lines are produced given the properties of the ambient plasma and their relative intensities. Clearly, both types of atomic data are needed to describe the observed line features. The first provides the particle, the second the photon mix.

Calculation of the atomic data in many cases is difficult or very time consuming. Relativity cannot be neglected in intermediate-Z ions so that intermediate coupling must be used to describe the atomic structure. The proper predictions of ionization and recombination rates involve many processes such as resonant excitation-autoionization, recombination into metastable levels, etc., that are more often than not missing from calculations. Nevertheless, these calculations are arguably still less complex than those necessary for proper prediction of the X-ray emission from a given ion species. The latter not only must include line formation by recombination and ionization phenomena, but also radiative cascades from higher-lying levels, resonance excitation, radiative decay by higher-order multipoles, and collisional deexcitation, among others. Because of this complexity, most calculations compute only a fraction of the entire problem. Even then, they must rely on approximations.

The need for laboratory measurements is clear. Again and again laboratory data have shown that calculations are incomplete, i.e., that they are missing crucial physics left out as part of the approximations. And laboratory data provide the yard stick by which to determine the accuracy of calculations. They are used as means to decide when a given calculational result is “good enough”, i.e., when to break off a time-consuming calculation.

The conventional approach in laboratory measurements has been to measure a given cross section, wavelength, or rate and compare it with theory. While this approach, which simply isolates a single piece of a very complex puzzle, is standard in atomic physics, it does not work for laboratory astrophysics. Approaches are needed that address a whole set of processes working together and cover the whole spectrum. Advances in experimental design during the past decade have allowed such measurements. New generation atomic physics devices have been developed that act as “analog computers” providing the data needed to describe X-ray spectra in detail. These devices are: (1) merged and crossed beam facilities for the measurement of ionization cross sections, (2) ion storage ring facilities for the measurement of ionization cross sections and low-energy dielectronic recombination resonances, (3) late-generation synchrotrons for photoionization measurements, and (4) electron beam ion traps for measurements of electron-ion excitation cross sections and high-energy dielectronic recombination resonances.

The new laboratory devices have in common that large sets of atomic data can be generated in a rather short amount of time. No longer is it necessary to measure one small piece of the puzzle over a long period of time. Once the experimental conditions are set up, say for measuring dielectronic recombination, much of the same data can be produced in a relatively short time. For example, by sweeping the energy of the electron cooler in a storage ring all dielectronic resonances can be measured for a given ion that fall into the energy range accessible with the electron beam. Similarly, by sweeping the beam energy in the electron beam ion trap all excitation processes contributing to a given line can be measured. The new generation machines thus contrast starkly with older plasma sources such as sparks and lasers, where most of the experimental time is spent understanding the source itself. The new devices are ready to go on demand and can thus truly function as analog computers that can generate the desired data more accurately than computer codes do. Moreover, the new sources operate in a low-density regime so that the data are directly applicable to most astrophysical plasmas.

Unlike computer codes, controlled measurements can in principle account for all processes. None of the physics is left out. For example, if the Breit-interaction is relevant for a given dielectronic resonance, it is included when the resonance is measured. If quantum electrodynamics shifts a given line position, it will show up in the spectrum. If relativity turns on a particular radiative decay mode, the line will automatically appear in the spectrum. If configuration interaction influences the line intensity, the line intensity will reflect that intensity. If cascade contributions from thousands of levels need to be summed to get the correct flux of a line, the sum will automatically be “computed” in the measurement.

Of course, no measurement is perfect. Setting up the appropriate measurement technique is paramount to measuring the correct quantities with the desired accuracy. When done appropriately, serious measurements provide an invaluable parameter: reliable uncertainty limits. Uncertainty limits are something very few calculations can provide.

One may argue that the combination of being able to generate large amounts of experimental data on demand and to give uncertainty estimates reduces the reliance on calculations and in many cases eliminates it. For example, by using the merged beam technique ionization cross sections for virtually all charge states of iron have been measured in the range below 2 keV and for some as high as 5 keV (Müller 1991, Stenke et al. 1999a,b). Storage rings have refined such measurements so that even minute contributions from exotic processes are included with high accuracy in the measurements

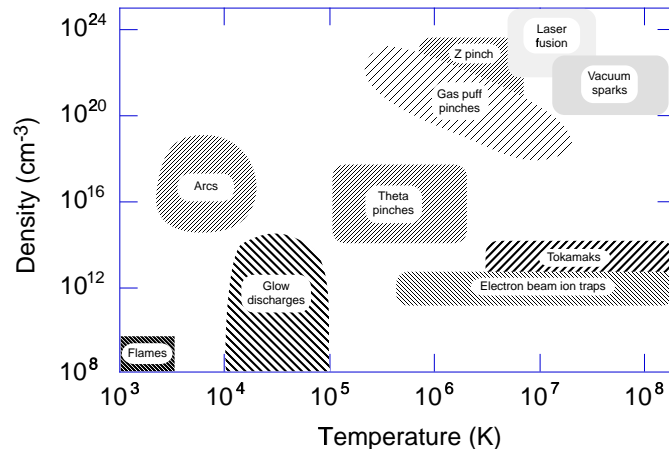


Figure 1. Density and temperature space sampled by different spectroscopic light sources. The EBIT source provides the appropriate charge states found in astrophysical plasmas at densities comparable to stellar atmospheres. Storage rings and merged beam apparatuses are not shown, as they do not generally provide spectroscopic data.

(Linkemann et al. 1995). Similarly, storage rings can measure low-energy recombination rates, both due to dielectronic and radiative capture, for virtually all ions (Andersen et al. 1992; Schuch et al. 1997; Müller et al. 1998). The electron beam ion trap can measure virtually all high-energy dielectronic recombination rates (Beiersdorfer et al. 1992a,b; Knapp et al. 1993). Although not all of these rates have indeed been measured, this nevertheless means that the relevant cross sections and rates that enter charge balance calculations can be measured with existing laboratory apparatuses. Reliance on theoretical cross section calculations could be eliminated in the near future, provided resources were focused on making the necessary measurements.

In the following, we describe measurements performed with the electron beam ion trap (EBIT) at Livermore. Unlike merged beams and storage rings, which measure ionization and recombination by detecting changes in the ion charge, the EBIT measures the radiation emitted by the ions. The data produced by EBIT is thus most closely related to that observed by X-ray missions. In fact, among laboratory sources of X radiation, the EBIT source is the closest in parameter space to those of hot astrophysical X-ray emitting plasmas, as illustrated in Figure 1. Only tokamak sources produce similarly high charge states at relatively low densities; but these plasmas lack the control afforded by the EBIT source. The conditions under which astrophysical spectra are produced can vary considerably – from ionizing plasmas in super nova remnants to stellar coronae in equilibrium and recombining photoionized plasmas surrounding accretion sources. Similarly, spectra at the LLNL EBIT source can be produced under many different conditions that simulate those of astrophysical sources. This allows us not only to measure specific atomic rates but also to test the interplay of different line formation processes. The source thus offers tremendous versatility not found in other laboratory plasmas.

2. The EBIT Source

The electron beam ion trap was designed and implemented at the Lawrence Livermore National Laboratory. It was specifically developed and built for studying the interactions of electrons with highly charged ions using X-ray spectroscopy (Levine et al. 1989). A schematic of the device is shown in Figure 2. Neutral atoms or ions with low charge are injected into a nearly monoenergetic beam where they are collisionally ionized and excited by an electron beam. The beam electrons are confined and focused by a 3 Tesla magnetic field, generated by a pair of superconducting Helmholtz coils. As the beam passes through the trap region of 2-cm length, it is compressed to a diameter of approximately 60 μm . Ions are longitudinally confined in the trap by applying the appropriate voltages to a set of three drift tubes

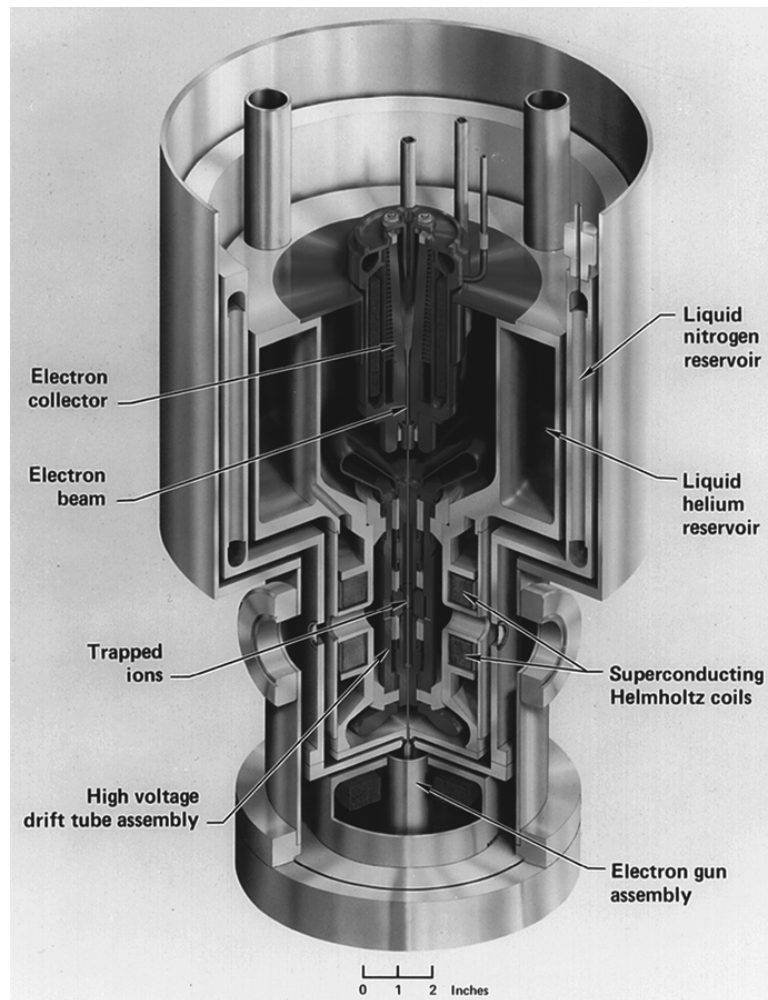


Figure 2. Artist's view of the EBIT device developed and deployed at Livermore.

through which the beam passes. Radial confinement is provided by electrostatic attraction of the electron beam, as well as flux freezing of the ions within the magnetic field. All three drift tube voltages float on top of a common potential that is supplied by a fast-switching high-voltage amplifier. The electron beam energy is determined by the sum of these potentials and may range between about 150 and 20,000 eV for most measurements of interest. The electron beam density at a given beam energy can be selected by varying the beam current. It typically is in the range of $2 \times 10^{11} - 5 \times 10^{12} \text{ cm}^{-3}$, i.e., in the range of many stellar coronae.

Six axial slots cut in the drift tubes and aligned with six vacuum ports permit direct line-of-sight access to the trap, as shown in Figure 3. One port is used for introducing atomic or molecular gases into the trap by means of a ballistic gas injection system. The remaining five ports are used for spectroscopic measurements. A seventh port on the top of EBIT permits axial access to the trap and is used for the injection of singly charged metal ions into the trap from a metal vapor vacuum arc source.

In over a decade of operation, spectroscopic instrumentation has been developed that matches the unique properties of the source. This instrumentation now provides measurements that span the 1 – 7000 Å region, i.e., the region from X rays to the visible. Special emphasis was placed on the X-ray and EUV regions to provide laboratory data for astrophysics missions such as *ASCA*, *Chandra*, *EUVE*, *DXS*,

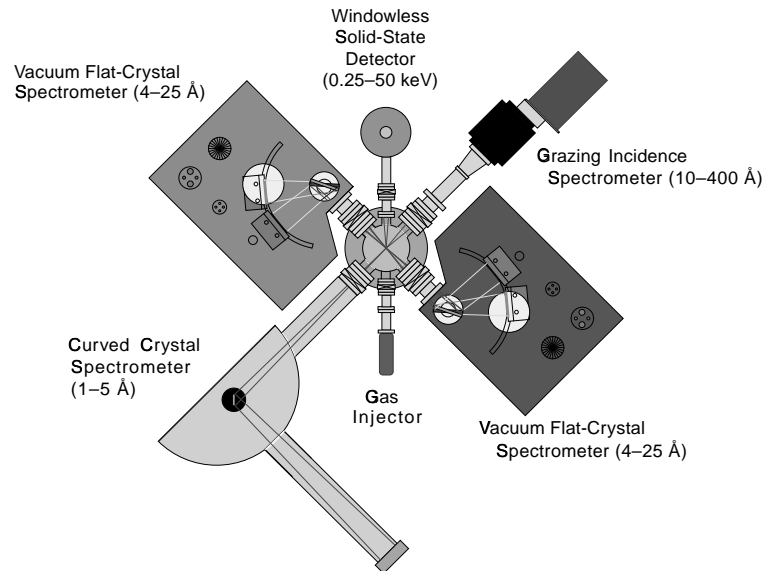


Figure 3. Radial cut through EBIT showing the six ports that provide access to the trap. Five ports are used for spectroscopy. The sixth port is used to inject gases into the trap.

and *XMM*. A typical arrangement for X-ray astrophysics is shown in Figure 3. A windowless high-purity Ge detector monitors the overall X-ray emission from the ions. This signal is used for tuning the facility, for count rate normalization, and for monitoring the presence of impurity ions. Two high-resolution bent-crystal spectrometers are available to provide detailed information on K-shell line emission spectra below 5 Å (Beiersdorfer et al. 1990). Two flat-crystal spectrometers operating *in vacuo* provide detailed L-shell and K-shell spectra in the 4 – 25 Å region (Brown et al. 1999). Two flat-field spectrometers, one with a 1200 ℓ/mm , the other with 2400 ℓ/mm grating are used to study the 10 – 400 Å extreme ultraviolet region (Beiersdorfer et al. 1999a). An X-ray calorimeter with parameters identical to those of the X-Ray Spectrometer (XRS) that had been part of the *Astro-E* mission will commence operation in summer 2000.

We use multichannel detection to increase efficiency and provide data of the highest level of reliability. X-ray detectors include gas-proportional counters, CCD cameras, and microchannel plates. Data are recorded with a multi-parameter data acquisition system.

A very important feature of EBIT is the ability to produce ions of a desired charge state. We do so by relying on the fact that we can choose the energy of the electron beam. This provides us with a powerful technique to determine which line comes from which ionization state. A calculation of the iron ionization balance as a function of electron beam energy based on electron-impact ionization and radiative recombination is shown in Figure 4.

Proper selection of the beam energy also allows us to select a specific line formation process. In fact, excitation processes are best studied by sweeping the energy of the electron beam in a continuous fashion after the desired ion balance has been established. The multi-parameter data acquisition system allows us to tag each X-ray event with the energy of the electron beam. This procedure correlates the line emission to specific beam energies and to determine the excitation function of a given spectral line. Resonant enhancement in the line emission, onsets of radiative cascades from higher levels, and dielectronic satellite features blending with a given line can thus be measured and the relative magnitude of each process assessed for different electron energies, as discussed in subsequent sections.

A novel and very useful feature is the ability to sweep the electron beam energy in time so as to reproduce a Maxwellian electron distribution function. To do so we have developed a procedure for rapidly changing the energy of the electron beam using a programmable arbitrary function generator. At the same time the current is adjusted to keep the electron density constant. Typical traces of electron

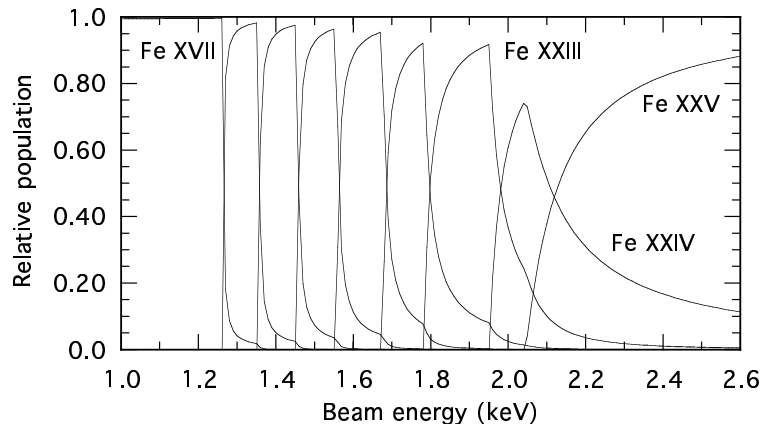


Figure 4. Calculated iron ionization balance in EBIT as a function of electron beam energy.

beam energy and beam current are given in Figure 5. When integrated over one sweep period this provides nearly the same electron energy distribution function as that found in a Maxwellian plasma of a given temperature. Missing are only very low and very high energy electrons, as we can set the beam energy neither to zero nor to infinity. Luckily such truncations are unimportant for most X-ray applications (cf. Savin et al. 1999). The sweeping is done fast enough so that the ionization equilibrium has no time to adjust to the instantaneous beam conditions but sees only the average that represents the Maxwellian temperature. The great advantage of this procedure is that we can dial up any given

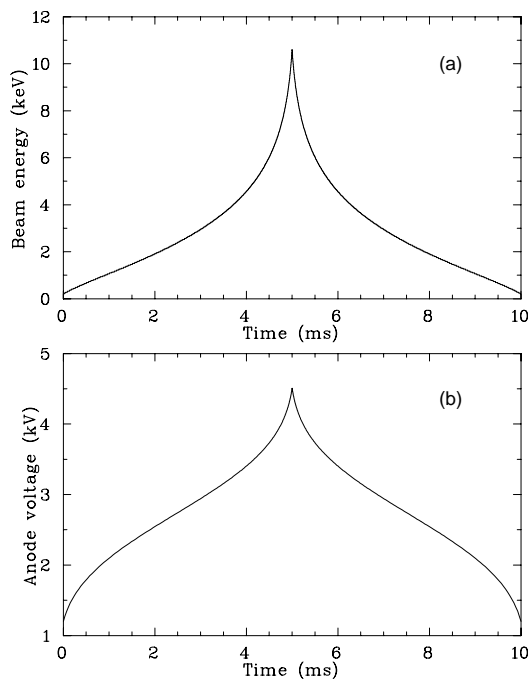


Figure 5. Timing patterns used to simulate a Maxwellian plasma with EBIT: (a) electron beam voltage, (b) voltage on the electron gun anode producing the beam current. The traces simulate a 2.0 keV plasma.

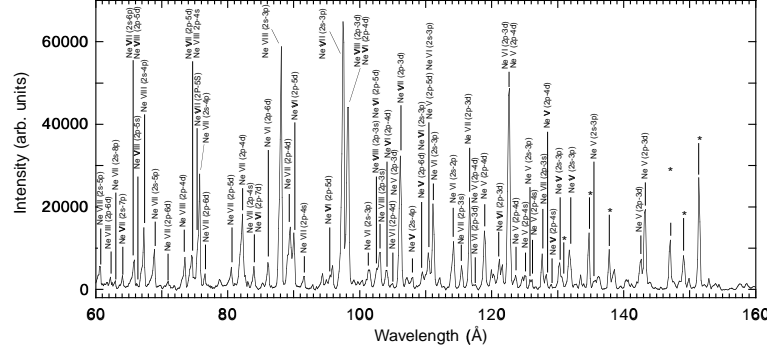


Figure 6. Spectrum of Ne v – Ne VIII. Lines are identified by the charge state and the transition. Lines marked (*) are second order lines.

temperature and produce the relevant spectra. EBIT truly acts as an analog computer that calculates the spectra for us.

3. Representative EBIT Measurements of M-shell, L-shell, and K-shell Spectra

The extreme ultraviolet wavelength band can be observed with *Chandra* up to 200 Å. This overlaps with the range covered by the short-wavelength spectrometer aboard the *EUVE* satellite. Using our 1200 ℓ/mm grating spectrometer we have surveyed the emission from four charge states of neon in this wavelength band. A typical spectrum is shown in Figure 6. The spectrum shows the sheer wealth of lines. Clearly, these lines represent a great potential for detailed plasma diagnostics provided all lines are properly accounted for in the spectral models.

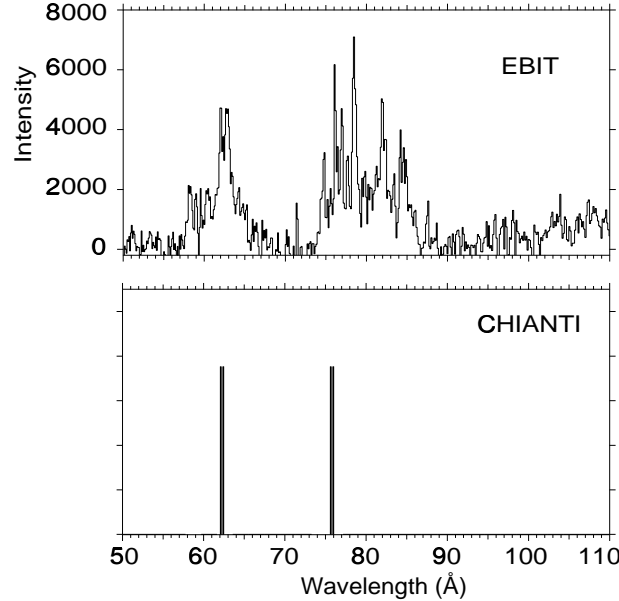


Figure 7. Spectrum of Fe XIII in the extreme ultraviolet: (a) measurement on EBIT; (b) predictions from the CHIANTI data base. CHIANTI does not give intensities for the four lines it lists, so the lines shown indicate no more than their positions.

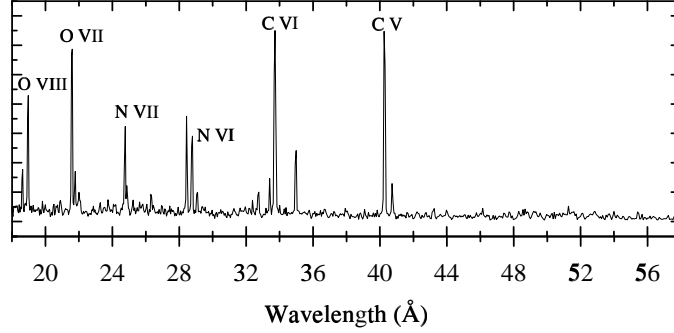


Figure 8. K-shell emission from carbon, nitrogen, and oxygen in the extreme ultraviolet recorded with EBIT.

Using the same instrumentation, we have performed systematic measurements of the M-shell emission of Fe VII through XVI in the 60–140 Å region. Much of this emission is unknown. To illustrate this point, we show a spectrum of Fe XIII in Figure 7 and compare it to the data found in CHIANTI (Dere et al. 1997). The comparison demonstrates the incompleteness of the modeling data base. This lack of data is not just a problem of CHIANTI; it extends to all data bases, including MEKA (Kaastra et al. 1993) and the Arcetri model (Landini and Monsignori Fossi 1990). The problem spans across all charge states of iron from Fe XIII and below (Lepson et al. 2000). In fact, many of the problems in performing global fits to the short-wavelength spectra obtained by the *EUVE* mission (Mewe et al. 1995) appear be attributable to the fact that many of the lines are simply missing from the models used for the fits (Beiersdorfer et al. 1999b).

The shorter wavelength region below 60 Å is accessed with our 2400 ℓ/mm grating. A spectrum of the K-shell emission from heliumlike and hydrogenic ions of the CNO group is shown in Figure 8. This region is especially important for such missions as *DXS*, *Chandra*, and *XMM*.

Yet shorter wavelengths are analyzed on EBIT with crystal spectrometers. Using our two flat crystal spectrometers, we are able to measure the entire emission from L-shell iron ions in the 10 – 18 Å region simultaneously (Brown et al. 1998, 1999). A spectrum of the Fe XVII emission is shown in Figure 9. Although the spectrum is better known than M-shell, new lines are identified. The new lines are relatively weak and are mostly transitions from levels with high principal quantum number n . However, because most of these lines are clustered near the ionization limit for Fe XVII, these high- n L-shell transitions contribute to a narrow part of the spectrum between about 10 – 11 Å. The combined flux of these lines is about 13 % of that of the strong $3d \rightarrow 2p$ resonance line at 15.0 Å. This is a considerable

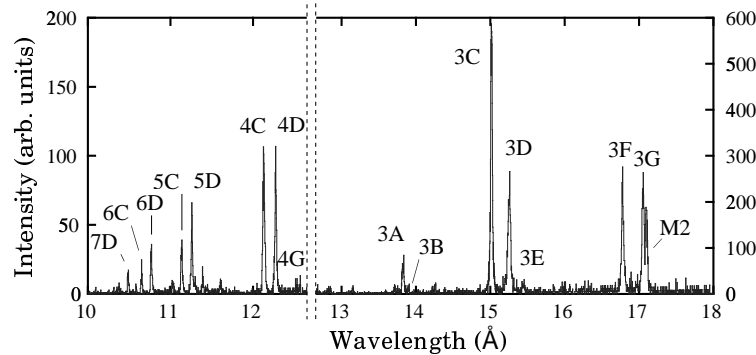


Figure 9. L-shell emission spectrum of Fe XVII. The range shown is the full range simultaneously accessible with our flat-crystal spectrometers. Note that there are different vertical scales associated with the left and right halves of the spectrum.

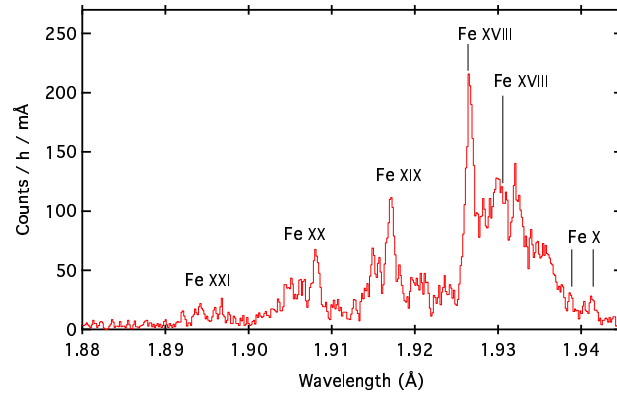


Figure 10. K-shell spectrum of Fe x – Fe xx. The emission in the range from 1.925 to 1.940 Å is comprised of K-shell lines from all charge states of iron between Fe xvii and Fe x. Individual contributions cannot be resolved and are not marked except for the four features shown.

amount of flux that has not been included in most spectral codes. A study of the contributions from these high- n transitions on the spectrum of Capella observed with *ASCA* was made recently (Brickhouse et al. 2000) and found to be a significant effect.

Spectra have also been measured for all higher charge states of iron in this wavelength band. Many lines have been identified for the first time (e.g., Drake et al. 1999). A preliminary line list of the L-shell

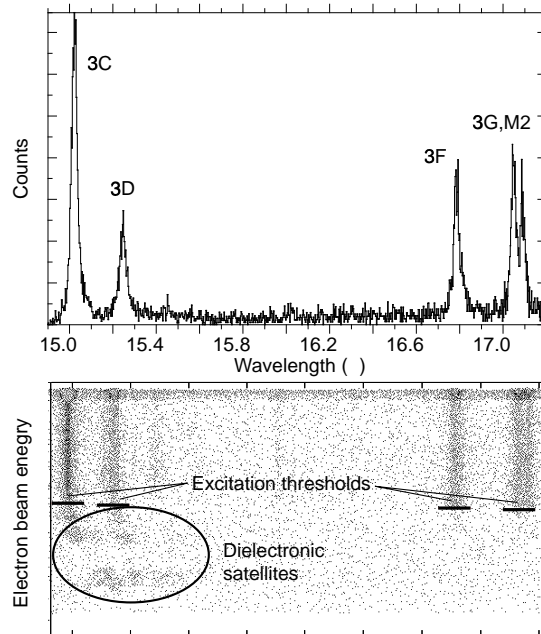


Figure 11. Emission of the $3d \rightarrow 2p$ and $3s \rightarrow 2p$ transitions in neonlike Fe xvii. The bottom figure shows the emission as a function of electron energy. The threshold for direct electron-impact excitation is marked. Emission below threshold is due to dielectronic satellites.

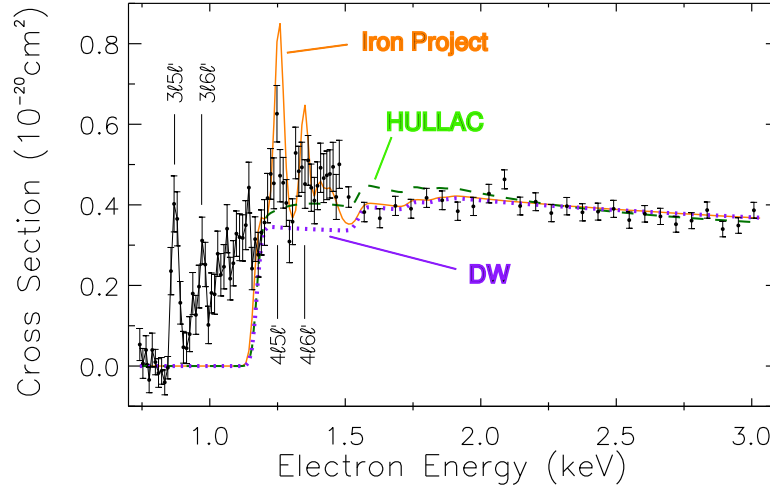


Figure 12. Emission of the $3p_{3/2} \rightarrow 2s_{1/2}$ transition in lithiumlike Fe^{23+} as a function of electron energy showing dielectronic satellite contributions below threshold and resonance excitation contributions above threshold for electron-impact excitation. Different theoretical predictions are indicated: HULLAC (Gu et al. 1999); Iron Project (Berrington and Tully 1997); DW (Zhang et al. 1990).

iron lines from Fe XVIII through Fe XXIV was published in (Phillips et al. 1999). A more comprehensive list is in preparation (Brown et al. 2000). This list now contains about twice as many lines as were used in the MEKA model or were given in standard line lists.

The K-shell iron emission is very important for hot astrophysical sources such as galaxy clusters and supernova remnants. Using our high-resolution bent crystal spectrometers we have made numerous observations of the K-shell spectrum of iron. The spectral resolving powers in these measurements range from 800 to 20,000. Most of the lines from the higher charge states of iron in this spectrum are known. However, many of the lines from the lower charge states are not as well known, mostly because it is very difficult to produce low charge states of iron in the laboratory yet have the high electron energies needed to excite the K-shell lines. We have overcome these problems and measured the K-shell emission from very low charge states of iron, ranging from Fe XX to as low as Fe IX. A typical spectrum of the K-shell emission from low charge state iron ions is shown in Figure 10. Line lists resulting from our K-shell measurements can be found in (Beiersdorfer et al. 1993, Decaux et al. 1995, 1997).

4. Determination of Line Formation Processes and Excitation Cross Sections

Line identification is only a small, albeit important, part of our measurements. Using the ability to quickly switch the electron beam energy, we map out different line formation processes. Such processes include both direct electron-impact excitation as well as indirect line formation processes, such as those associated with resonance excitation and high- n dielectronic satellite contributions.

As an example of the different line formation processes contributing to a given line we show in Figure 11 the L-shell lines from Fe XVII in the 15 – 18 Å range. By sweeping the electron beam energy from as low as 200 eV to well above 2000 eV, the measurement identifies the different contributions to the lines: direct electron-impact excitation and resonance excitation above the threshold for excitation, and dielectronic-recombination satellite lines below threshold. While the latter are technically lines different from their parent line, they cannot be resolved and contribute to the line intensity observed in a plasma source. The figure immediately shows that dielectronic resonances are important for the $3d \rightarrow 2p$ lines. But dielectronic resonances are not important for the $3s \rightarrow 2p$ lines.

Based on such energy-dependent measurements the excitation cross section contributing to given line as a function of energy can be readily extracted. An example for the $3d_{5/2} \rightarrow 2p_{3/2}$ transition in lithiumlike Fe XXIV is shown in Figure 12.

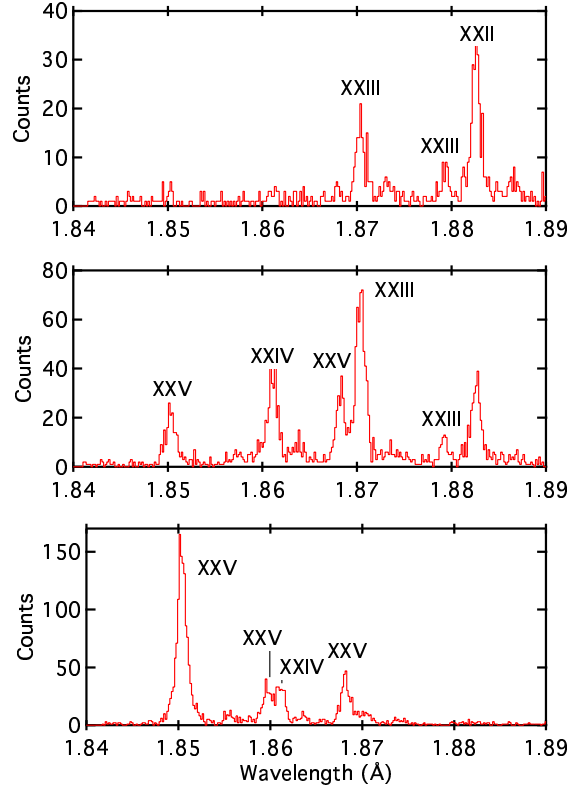


Figure 13. K-shell emission from iron ions for different values of the ionization parameter $\eta = n_e t$: (a) $\eta = 5 \times 10^{10} \text{ cm}^{-3}$, (b) $\eta = 20 \times 10^{10} \text{ cm}^{-3}$, (c) $\eta = 50 \times 10^{10} \text{ cm}^{-3}$. Lines strongly enhanced by innershell ionization are the Fe XXIII line at 1.879 Å and the Fe XXV line at 1.868 Å. These can be used as markers for ionizing plasmas for high values of η .

As noted, the contributions from the dielectronic satellite lines, especially those that are unresolved in wavelength from their parent line, are important for accounting for all of the flux. Our measurements show that such satellites can enhance some L-shell lines in Fe XXIV by 20 % (Gu et al. 1999) or more, especially in colder plasmas. As already illustrated in Figure 12, we stress that not all lines are enhanced by such contributions. Each line must be treated individually. This counters the assumptions made in the MEKA model, for example, where essentially every electron-dipole-allowed line is assumed to have a given percentage of the flux emanating from dielectronic satellites.

5. Nonequilibrium Processes

Many astrophysical plasmas are not in charge-balance equilibrium. Our capabilities that allow us to rapidly switch the energy of the electrons also let us simulate nonequilibrium conditions. For example, we have simulated ionizing plasmas found in super nova remnants by studying the time dependence of the spectral emission as charge state equilibrium is reached (Decaux et al. 1997). Such a simulation allows us to identify various markers for ionizing plasmas among the iron K lines. Typical spectra of the K-shell iron emission for different values of the ionization parameter $\eta = n_e t$ are shown in Figure 13.

Recombining plasmas are another area of investigation. In photo-ionized plasmas, high charge state ions are produced in intense photon fields. The electron temperature is rather low, and the role of electrons in X-ray line formation is purely limited to recombination. We have simulated such conditions

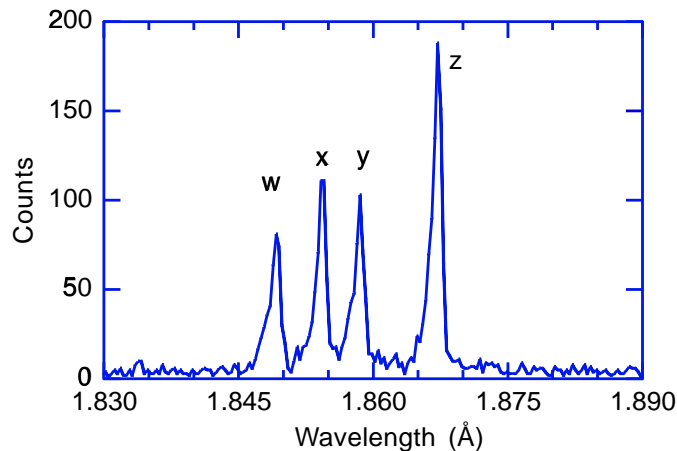


Figure 14. K-shell emission from iron produced by electron capture. All emission is from Fe xxv ions. The lines are labeled in the following notation: $w - 1s2p\ ^1P_1 \rightarrow 1s^2$, $y - 1s2p\ ^3P_1 \rightarrow 1s^2$, $x - 1s2p\ ^3P_2 \rightarrow 1s^2$, $z - 1s2s\ ^3S_1 \rightarrow 1s^2$. No lower charge states may contribute. Such spectra are produced in photo-ionized plasmas.

by first producing a given ionization state, then switching the energy of the electrons to values where recombination is the only line formation process. A typical K-shell spectrum of Fe xxv produced by electron capture into hydrogenic Fe xxvi ions is shown in Figure 14. The spectrum looks very different from that produced in a hot electron plasma. The triplet lines are much stronger than the singlet lines, which is in stark contrast to spectra produced by electron-impact excitation. Furthermore, no satellite transitions, neither collisional nor dielectronic, from lower charge states are visible. The latter is the result of the fact that none of the lower charge states has a K-shell vacancy, thus precluding the possibility that a K-shell transition takes place during the recombination process. This makes the spectra unique for identifying recombination dominated plasmas.

6. Conclusion

Facilities nowadays exist that can produce much of the atomic data needed for the proper and reliable interpretation of astrophysical X-ray data. Ionization and recombination cross sections for all astrophysically relevant ions can be measured by using particle-counting techniques on storage rings and crossed and merged beam facilities. Such measurements include resonance phenomena that may lead to double ionization or that enhance recombination. Similarly, X-ray excitation cross sections can be measured by observing the spectra of interest directly in the laboratory by using photon counting techniques on the EBIT. X-ray spectroscopic measurements at the Livermore EBIT have been optimized over the past decade to provide definitive values of electron-impact excitation, dielectronic and resonance excitation cross sections. By looking directly at the processes that produce line emission, the EBIT measurements can assess whether or not a particular process is relevant and which lines need to be included in spectral models. The Livermore measurements now cover the entire K-shell or L-shell complex in essentially one experimental setup and can provide the atomic data needed for synthesizing accurate spectral models. Most importantly, the spectral and collisional data provided by the new facilities provide uncertainty limits that are invaluable in establishing believable bounds on the physical parameters inferred from spectroscopic observations of astrophysical data.

Acknowledgments. Discussions with Duane Liedahl, Nancy Brickhouse, and Mau Chen are gratefully acknowledged. This work was supported by NASA grants NAG5-6731 and NAG5-5123 and work order W-19127 and was performed under the auspices of the Department of Energy by the University of California Lawrence Livermore National Laboratory under contract No. W-7405-ENG-48.

References

- Andersen, L. H., Pan, G. Y., Schmidt, H. T., Pindzola, M. S., and Badnell, N. R. 1992, *Phys. Rev. A* 45, 6332.
- Beiersdorfer, P., Lepson, J. K., Brown, G., Utter, S. B., Kahn, S., Liedahl, D., and Mauche, C. W. 1999b, *Astrophys. J.* 519, L185.
- Beiersdorfer, P., López-Urrutia, J. R. C., Springer, P., Utter, S. B., and Wong, K. L. 1999a, *Rev. Sci. Instrum.* 70, 276.
- Beiersdorfer, P., Marrs, R. E., Henderson, J. R., Knapp, D. A., Levine, M. A., Platt, D. B., Schneider, M. B., Vogel, D. A., and Wong, K. L. 1990, *Rev. Sci. Instrum.* 61, 2338.
- Beiersdorfer, P., Phillips, T., Jacobs, V. L., Hill, K. W., Bitter, M., von Goeler, S., and Kahn, S. M. 1993, *Astrophys. J.* 409, 846.
- Beiersdorfer, P., Phillips, T. W., Wong, K. L., Marrs, R. E., and Vogel, D. A. 1992a, *Phys. Rev. A* 46, 3812.
- Beiersdorfer, P., Schneider, M. B., Bitter, M., and Von Goeler, S. 1992b, *Rev. Sci. Instrum.* 63, 5029.
- Berrington, K. A., and Tully, J. A. 1995, *Astron. & Astrophys.* 126, 105.
- Brickhouse, N. S., Dupree, A. K., Edgar, R. J., Liedahl, D. A., Drake, S. A., White, N. E., and Singh, K. P. 2000, *Astrophys. J.* 530, 387.
- Brown, G., Beiersdorfer, P., Kahn, S., Liedahl, D., and Widmann, K. 1998, *Astrophys. J.* 502, 1015.
- Brown, G. V., Beiersdorfer, P., Liedahl, D. A., Widmann, K., and Kahn, S. M. 2000 (in preparation; available as LLNL preprint UCRL-JC-136647).
- Brown, G. V., Beiersdorfer, P., and Widmann, K. 1999, *Rev. Sci. Instrum.* 70, 280.
- Decaux, V., Beiersdorfer, P., Kahn, S. M., and Jacobs, V. L. 1997, *Astrophys. J.* 482, 1076.
- Decaux, V., Beiersdorfer, P., Osterheld, A., Chen, M., and Kahn, S. M. 1995, *Astrophys. J.* 443, 464.
- Dere, K. P., Landi, E., Mason, H. E., Fossi, B. C. M., and Young, P. R. 1997, *A&AS* 125, 149.
- Drake, J. J., Swartz, D. A., Beiersdorfer, P., Brown, G. V., and Kahn, S. M. 1999, *Astrophys. J.* 521, 839.
- Gu, M., Kahn, S., Savin, D., Beiersdorfer, P., Brown, G., Liedahl, D., Reed, K., Bhalla, C., and Grabbe, S. 1999, *Astrophys. J.* 518, 1002.
- Kaastra, J.S., and Mewe, R. 1993, *Legacy* 3, 16.
- Knapp, D. A., Marrs, R. E., Schneider, M. B., Chen, M. H., Levine, M. A., and Lee, P. 1993, *Phys. Rev. A* 47, 2039.
- Landini, M., and Monsignori Fossi, B. C., *Astron. Astrophys. Suppl.* **82**, 229 (1990).
- Lepson, J. K., Beiersdorfer, P., Brown, G. V., Kahn, S. M., Liedahl, D. A., Mauche, C. W., and Utter, S. B. 2000, *Revista Mexicana de Astronomia y Astrofisica* 9, 137.
- Levine, M. A., Marrs, R. E., Bardsley, J. N., Beiersdorfer, P., Bennett, C. L., Chen, M. H., Cowan, T., Dietrich, D., Henderson, J. R., Knapp, D. A., Osterheld, A., Penetrante, B. M., Schneider, M. B., and Scofield, J. H. 1989, *Nucl. Instrum. Methods B43*, 431.
- Linkemann, J., Müller, A., Kenntner, J., Habs, D., Schwalm, D., Wolf, A., Badnell, N. R., and Pindzola, M. S. 1995, *Phys. Rev. Lett.* 74, 4173.
- Mewe, R., Kaastra, J.S., Schrijver, C.J., van den Oord, G.H.J., and Alkemade, F.J.M. 1995, *Astron. Astrophys. Suppl.* 296, 477.
- Müller, A. 1991, *Physica Scr.* T37, 14.
- Müller, A., Bartsch, T., Brandau, C., Hoffknecht, A., Knopp, H., Schippers, S., Uwira, O., Linkemann, J., Saghir, A. A., Schmitt, M., Schwalm, D., Wolf, A., Bosch, F., Franzke, B., Kozhuharov, C., Mokler, P. H., Nolden, F., Steck, M., Stohlker, T., Winkler, T., Danared, H., DeWitte, D. R., Gao, H., Lebius, H., Schuch, R., Spies, W., Zong, W., Dunn, G.H., Graham, W. G., Tanis, J. A., Doerfert, J., Savin, D., and Stachura, Z. 1998, *Hyperf. Inter.* 114, 229.
- Phillips, K. J. H., Mewe, R., Harra-Murnion, L. K., Kaastra, J. S., Beiersdorfer, P., Brown, G. V., and Liedahl, D. A. 1999, *Astron. Astrophys. Suppl.* 138, 381.

- Savin, D. W., Beck, B., Beiersdorfer, P., Kahn, S. M., Brown, G. V., Gu, M. F., Liedahl, D. A., and Scofield, J. H. 1999, *Phys. Scripta* T80, 312.
- Schuch, R., DeWitt, D. R., Gao, H., Mannervik, S., Zong, W., and Badnell, N. R. 1997, *Physica Scr.* T73, 114.
- Stenke, M., Aichele, K., Hartenfeller, U., Hathiramani, D., Steidl, M., and Salzborn, E. 1999a, *J. Phys. B* 32, 3627.
- Stenke, M., Hartenfeller, U., Aichele, K., Hathiramani, D., Steidl, M., and Salzborn, E. 1999b, *J. Phys. B* 32, 3641.
- Zhang, H. L., Sampson, D. H., and Fontes, C. J. 1990, *Atom. Data Nucl. Data Tables* 44, 31.